Study for removing of silica nanoparticle in pure isopropyl alcohol with a cation exchange membrane

Fujimura, Yu ; Kawakatsu, Takahiro ; Morimoto, Masayuki ; Asakawa, Hitoshi ; Nakagawa, Keizo ; Yoshioka, Tomohisa

(Citation)
Journal of Molecular Liquids,367(A):120441

(Issue Date)
2022-12-01

(Resource Type)
journal article

(Version)
Accepted Manuscript

Study for removing of silica nanoparticle in pure isopropyl alcohol with a cation exchange membrane

Yu Fujimura,[1,5,*] Takahiro Kawakatsu,[1] Masayuki Morimoto,[2,3] Hitoshi Asakawa,[2,3,4] Keizo Nakagawa,[5,6] and Tomohisa Yoshioka[5,6]

[1] Basic Technology R&D Group, Innovation Division, Kurita Water Industries Ltd., 3993-15 Haijima-cho, Akishima-shi, Tokyo 196-0002, Japan

[2] Nanomaterials Research Institute (NanoMaRi), Kanazawa University, Kakuma-machi, Kanazawa 920-1192, Japan

[3] Graduate School of Natural Science & Technology, Kanazawa University, Kakuma-machi, Kanazawa 920-1192, Japan

[4] Nano Life Science Institute (WPI-NanoLSI), Kanazawa University, Kakuma-machi, Kanazawa-shi, Kanazawa 920-1192, Japan

[5] Graduate School of Science, Technology, and Innovation, Kobe University, 1-1 Rokkodai, Nada, Kobe 657-8501, Japan

[6] Research Center for Membrane and Film Technology, Kobe University, 1-1 Rokkodai, Nada, Kobe 657-8501, Japan

Keywords: Silica nanoparticle; Cation exchange membrane; Tentacle effect; Atomic force microscopy; Molecular dynamics; Zeta potential

*Corresponding: y.fujimura95@kurita-water.com

Abstract

Semiconductors are becoming increasingly miniaturized and structurally complex. During their manufacture, isopropyl alcohol (IPA), which has a low surface tension, is often used to prevent structural corruption during cleaning. A previous study examined the removal of impurities (silica nanoparticles (SNPs)) in IPA/water solutions using an anion exchange membrane and reported the removal mechanism. That study found that SNP removal in high ratio IPA was difficult. In the present study, SNP removal in IPA was tested using three different cation exchange membranes, and the differences in their removal performance were evaluated. Zeta potential measurements and molecular dynamics (MD) simulations were performed to elucidate the removal mechanism, and membrane

surface-SNP interactions were evaluated by atomic force microscopy (AFM). The zeta potential of the cation exchange membrane in IPA was positive. The reason for this phenomenon is discussed based on the results of MD simulations. The results suggested that Na^+, which is the counter ion in the ion exchange group, remains near the membrane surface. The difference in the removal ratio between the cation exchange membranes was examined by AFM, suggesting that the tentacle effect of the graft chains on the surface suppressed the re-desorption of SNPs once adsorbed, contributing to the high removal ratio. These results are expected to contribute significantly to developing membranes with a high removal ratio of SNPs in IPA.

1. Introduction

The transistor, which was invented at AT&T Bell Labs in 1947, has brought great benefits to the world and promoted the information society. The personal computer and the smartphone that emerged from this invention have become indispensable tools in contemporary business. Among these, semiconductors occupy an essential position and have evolved remarkably. Although they are now deviating from Moore's law [1], extensive research on new materials, miniaturization, and the development of 3D devices is being conducted to improve their performance [2–6]. Because the technology node has reached 3 nm and the structure has become very complex [2–4,6–9], not only ultrapure water, but also liquid IPA [10–14], which has a lower surface tension, is employed for wafer cleaning. This is to prevent the complex structure from disruption by the surface tension of cleaning liquid. The International Roadmap for Devices and Systems (IRDS) indicates that the control standard for particulates in IPA should be less than 50 particles/L for 50 nm or smaller particles [15]. A previous study [16] examined the removal mechanism of silica nanoparticles (SNPs) in IPA/water solutions using an anion exchange membrane by experiment, analysis, and simulation. These results provided important insights into SNP removal in water/IPA. On the other hand, SNPs cannot be removed at high IPA ratios using an anion exchange membrane due to the influence of Cl^- ions, which are counter ions of anion exchange groups. Using these insights, a new removal mechanism was assumed to achieve a high removal ratio of SNPs in IPA, applying an opposite concept of the removal mechanism of SNPs in water. As a removal material, a cation exchange membrane that generally had the same charge as SNPs was employed for the removal tests. Zeta potential measurements of a cation exchange membrane in IPA, MD simulations of ion behaviors, and Si-membrane force curve measurements using AFM were performed to elucidate the removal mechanism and consider optimal membrane structures. While previous studies evaluated only one type of membrane, this study compared the removal performance and the influence of the surface structure of the membranes of three different cation exchange

membranes and one anion exchange membrane. AFM measurements were performed to provide a more detailed evaluation of the effects.

2. Experimental, analysis, and simulation method

The following procedure is based on the method presented elsewhere [16], with slight modifications of the substances, concentrations, and models.

2.1. SNP removal in IPA

SNP removal tests in IPA were performed using ion exchange membranes. In this paper, removal tests were performed with four different ion exchange membranes and five different sizes of SNPs, and the removal ratios on each membrane were compared. Table 1 lists the three cation exchange membranes and one anion exchange membrane. The SNPs were 30, 50, 100, 300, and 1000 nm of Micromod Partikeltechnologie's sicastar®. The ion exchange membranes used for the test were 100 cm^2. The membrane was immersed repeatedly in IPA to displace the internal water content. After that, the immersed membrane was put into a solution inholding 10 ppm SNPs and shaken for 30 minutes. After the removal test, the solution was analyzed for the concentration of total silica by heat dissolution using sodium carbonate–molybdenum blue absorbance spectrophotometry, and the removal ratio was calculated. The equation for calculating the removal ratio is shown in Equation 1. Note that the SNP removal test with AMVN was performed only with the 30 nm SNP because the purpose of the test was to compare the SNP removal with CMVN, which has grafted chains.

Table 1 Membrane type used in the experiment

Name	Manufacture	Ion exchange group	Grafted chain	Size of SNPs used [nm]
Neosepta CMB	Astom	$–SO_3^-Na^+$	No	30, 50, 100, 300, 1000
Selemion™ CMTE	AGC	$–SO_3^-Na^+$	No	30, 50, 100, 300, 1000
Selemion™ CMVN	AGC	$–SO_3^-Na^+$	Yes	30, 50, 100, 300, 1000
Selemion™ AMVN	AGC	$–NR_3^+Cl^-$	Yes	30

$$Removal\ ratio\ [\%] = \frac{(C_{SNP}\ before\ test) - (C_{SNP}\ after\ test)}{(C_{SNP}\ before\ test)} \times 100 \quad \text{(Equation 1)}$$

2.2. Zeta potential and AFM measurement in IPA

The zeta potential measurement for the cation exchange membrane in IPA was performed with a Zetasizer Nano ZS (Malvern Panalytical), and ZEN1020 measurement cell. ZEN1020 cell is an optional equipment which allowed for the measurement a flat material. The membranes used were Neosepta CMB (Astom Corporation) and Selemion™ CMTE (AGC Corporation), and the tracer particles were 1 μm models of Micromod Partikeltechnologie's sicastar®. The concentration of tracer particles in the measurement was set to 1 ppm.

2.3. Force curve measurement with static-mode AFM

Force curve measurements with the static-mode AFM were performed to evaluate the interaction forces between the cation exchange membranes and SNPs in IPA. The Si cantilever (HQ:NSC19, MikroMasch, nominal spring constant: 0.5 N/m) with a guaranteed tip radius of less than 35 nm was used. Before the force curve measurements, the tip side was coated with 15 nm Si using a magnetron sputter coater (Q150TS, Quorum Technologies). The Si-coated tip was used as a model of SNPs because the coated Si layer was oxidized to form the thin silicon oxide layer in the air. Before the force curve measurements, the cation exchange membranes immersed in IPA were cleaned with ultrasonic treatment three times for 3 min.

Force curve measurements were performed using a laboratory-built atomic force microscope equipped with a commercially available AFM controller (ARC 2, Oxford Instruments). The AFM system was operated in static-mode to measure the interaction forces acting on the tip. The tip was scanned in the Z direction for 100 nm with a speed of 100 nm/s. The direction of tip scanning was inverted when the repulsive force acting on the tip reached 2.5 nN at the surface during the tip approach (Fig. 1a). Two thousand points of interaction forces were recorded in each approach and retract curves. The approach and retract force curves were collected by changing lateral positions over 700 points for each cation exchange membrane. The distances between the adjacent lateral positions were 15 nm.

Fig. 1b shows a typical force curve with frequent ruptures obtained at the CMVN surface in IPA. The sawtooth patterns originating from ruptures are observed in the retract curve. The retract force curves were analyzed to determine the rupture points (Fig. 1c). First, the maximum noise of each curve was defined as the threshold to eliminate the influence of noise in the rupture identification. The local minimum points were selected as candidates for rupture by comparing two proximal points on either side in the region of a more significant attractive force than the threshold. Finally, the candidate points were identified as ruptures when the difference between the candidate point and the proximal point on

the far side from the surface was more significant than the threshold value.

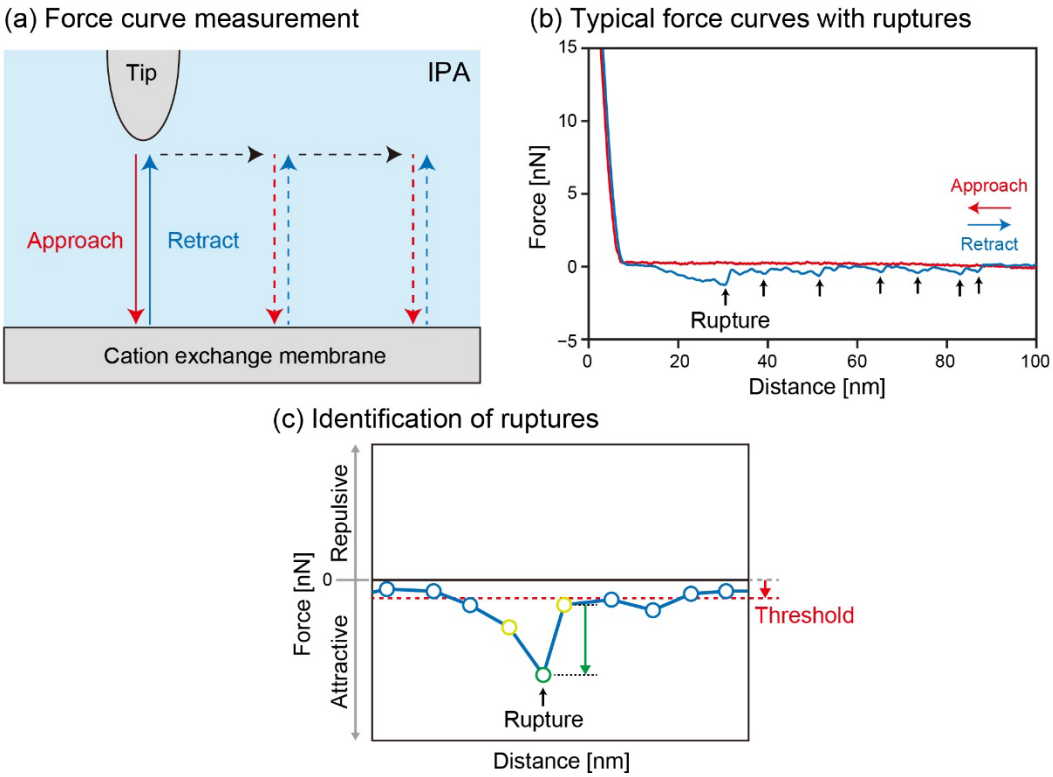

Fig. 1 Force curve measurement of cation exchange membranes in IPA

2.4. Molecular dynamics simulation

MD simulations were performed to investigate the difference in the changes in the position of the Na^+ ion, the counter ion of the cation exchange membrane, for IPA or water. The simulation software was BIOVIA Materials Studio® 2020. The Amorphous Cell module was used for membrane modeling and solvent molecule packing. The Forcite Plus module was used for structural optimization and for followed NVT (constant volume and temperature) and NPT (constant pressure and temperature) MD simulations. COMPASS II [17,18] was used for the force field; the potential functional forms are given in Supplementary Materials. The potential parameters and validation of COMPASS II are reported in [17] and [18], respectively. The validation of the properties using COMPASS II is reported elsewhere [19–21], which we consider appropriate for use in this simulation.

2.4.1. Membrane model

The cation exchange membranes used in the experiments in this paper are different in terms of the base material part. However, the basic structure related to ion exchange is a polymer based on Styrene-DVB monomer. Hence, there is no difference among the three types of cation exchange membranes shown in

Table 1 in terms of modeling. Because the DVB to styrene polymerization ratio is 7%–8% [22,23], monomer chains containing styrene and DVB in a mol ratio of 14:1 were formed, and 20 monomer chains and 280 counter ions of Na^+ ions were packed in a unit cell with d = 1.35 g/cc. The lattice parameter was set to $a = b$ = 60 Å, and c = 20.64 Å was automatically calculated based on the input density. Note that three-dimensional boundary conditions were applied to the unit cell for this study. After performing structural optimization calculations for the developed polymer model, NPT MD simulations[24,25] were conducted for 40 ps (Pressure = 2.0 GPa, Temperature = 298 K, and Time step = 1.0 fs). The unit cell size was determined to be $a = b$ = 59.91 Å, c = 20.61 Å, and the density was 1.36 g/cc. Bereandsen [26] was applied as the pressure adjustment/control method (a decay constant = 0.1 ps, and cutoff distance = 1.55 nm). Fig. 2 shows the chemical structural formula and the produced polymer model, and Table 2 lists the count of atoms in the monomer chain model and the membrane simulation model.

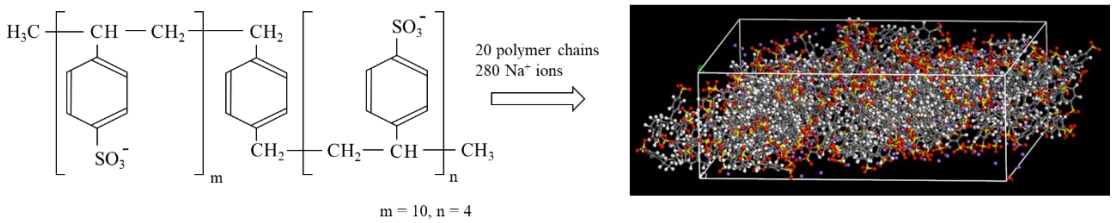

Fig. 2 The Styrene-DVB monomer model and the membrane simulation model (Atom or ion colors: white, H; gray, C; red, O; yellow, S; purple, Na^+)

Table 2 Count of atoms of simulation model

Kind of atom and ion	Styrene-DVB monomer chain model	Membrane simulation model
C	122	2440
H	112	2240
O	42	840
S	14	280
Na^+	14	280

The model developed in this study focuses on a limited part of the actual system, and it is hard to replicate the macroscopic physical properties of the ion exchange membrane. The physical properties of the ion exchange resin, which are closely related to the behavior, are important because the purpose of this simulation was to evaluate the behavior of Na^+ ions around the ion exchange group. The density of a typical cation exchange membrane ranged from 1.2 to 1.35 g/cc. Therefore, it is acceptable to

assume no significant deviation in density.

2.4.2. Model for evaluating the position of Na^+ ions

A 60 Å vacuum layer was installed on the membrane simulation model developed in the previous section, and H_2O and IPA molecules were packed in the empty space with 0.998 g/cc and 0.786 g/cc [27–29] as solvent molecules, respectively. The unit cell size was $a = b = 59.91$ Å and $c = 82.31$ Å, and three dimensional periodic boundary conditions were applied. Fig. 3 shows the simulation model with IPA as the solvent molecule. MD simulations under NVT ensemble conditions (298 K, Time step = 1.0 fs) were conducted for 1500 ps, and the position of the Na^+ ion, the counter ion of the cation exchange group, was evaluated at 0, 500, 1000, and 1500 ps.

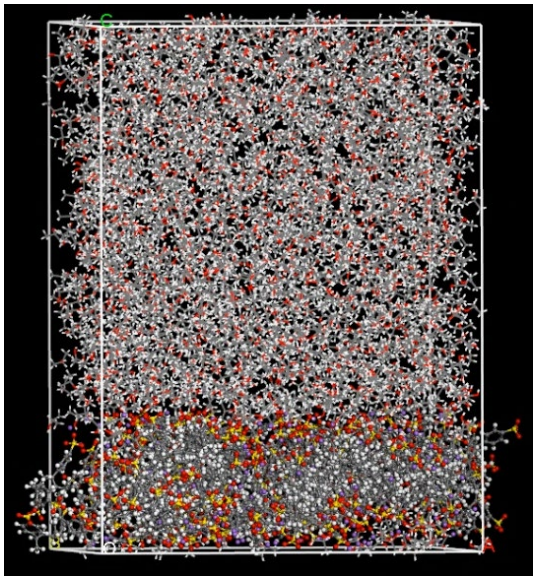

Fig. 3 Simulation model to evaluate the position of Na^+ ions in IPA (Atom and ion colors: white, H; gray, C; red, O; yellow, S; purple, Na^+)

3. Results and discussion about the mechanism of removal

3.1. Differences in SNP removal ratio between anion and cation exchange membranes

Fig. 4 shows the SNP removal ratio as a function of the SNP size. All cation exchange membranes could remove the smallest 30 nm SNP to some extent. The highest removal ratio of 72.17% was observed in the removal test of 30 nm SNP by CMVN. The removal ratio decreased with increasing SNP size for all cation exchange membranes, and an almost zero removal ratio was observed for the 1000 nm SNPs. On the other hand, the anion exchange membrane, AMVN, which has grafted chains as well as CMVN,

could not remove even the smallest 30 nm SNP. These results were consistent with a previous report [16]. CMB showed no removal performance for SNPs larger than 50 nm, and CMTE had a removal ratio of less than 5%, indicating that it had little removal performance. As for 30 nm SNPs, CMB had greater removal performance than CMTE (CMB: 29.35%, CMTE: 12.88%). To study the difference in the SNP removal performance of CMB and CMTE, the surface elemental properties of CMB and CMTE were measured by X-ray Photoelectron Spectroscopy, XPS (ULVAC Phi PHI 5000 Versa Probe II, JAPAN). The normalized values of S/C obtained by dividing the S atom composition of the functional group by the C atom composition of the base material were CMB: 7.48% and CMTE: 5.45%. From Fig. 4, the removal ratio for 30 nm SNPs is higher for CMB. Both membranes have a similar structure, but there is a difference in S/C. The higher S/C value for CMB suggests that it has a higher functional group density. Therefore, the 30 nm SNP removal ratio is CMB > CMTE. All XPS data were presented in Supplementary Materials.

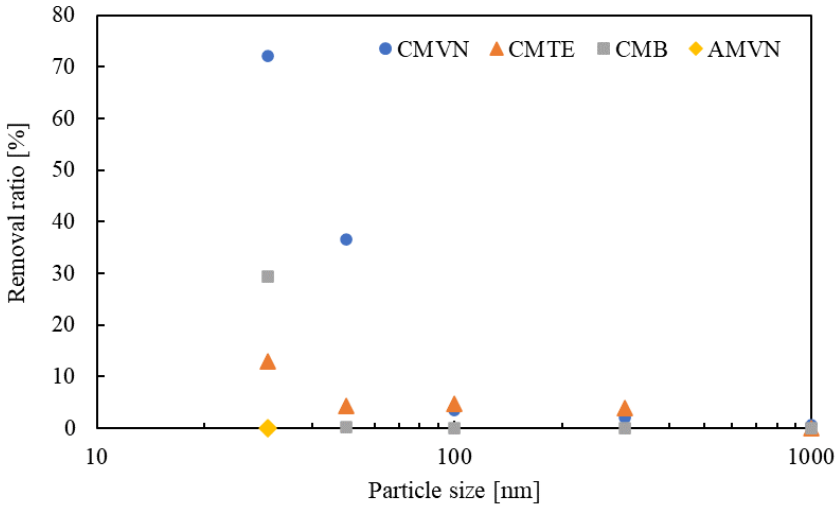

Fig. 4 SNP removal ratio of various sizes using each cation exchange membrane

Table 3 lists the zeta potential of the cation exchange membranes, Neosepta CMB and Selemion™ CMTE, an anion exchange membrane (Neosepta AHA), and SNPs in IPA. The zeta potential of the cation exchange membrane in IPA was positive, which is an opposite potential of a cation exchange membrane in water. The SNPs had a negative zeta potential, suggesting that SNPs could be removed by the interaction of opposite potentials of cation exchange membrane and SNPs. Since the absolute value of zeta potential is CMB > CMTE and the removal ratio for SNP size 30 nm in Fig. 4 is CMB > CMTE, it is assumed that the absolute value of zeta potential is correlated with the removal ratio. Note that we also tried to measure the zeta potential of CMVN, but the tracer particles, SNPs, were adsorbed and we could not obtain the data with reproducibility. On the other hand, anion exchange membranes

have negative zeta potentials in IPA. Therefore, anion exchange membranes could not remove SNPs because of the repulsive interactions between anion exchange membrane and SNPs.

Table 3 Zeta potential in IPA

Materials	Zeta potential in IPA [mV]
Neosepta CMB	7.39
Selemion™ CMTE	5.06
Anion exchange membrane*	−5.52*
SNP*	−3.75*

*Reference [16]

3.2. Simulating for evaluating the position of Na^+ ions

The reason for the positive zeta potential of the cation exchange membrane in IPA could be discussed from MD simulation results. Fig. 5 presents the change in the position of Na^+ ions (a-1 and a-2) and the local density distribution of Na^+ in the perpendicular direction to the membrane surface calculated for every 2 Å (b-1 and b-2) at 0, 500, 1000, and 1500 ps.

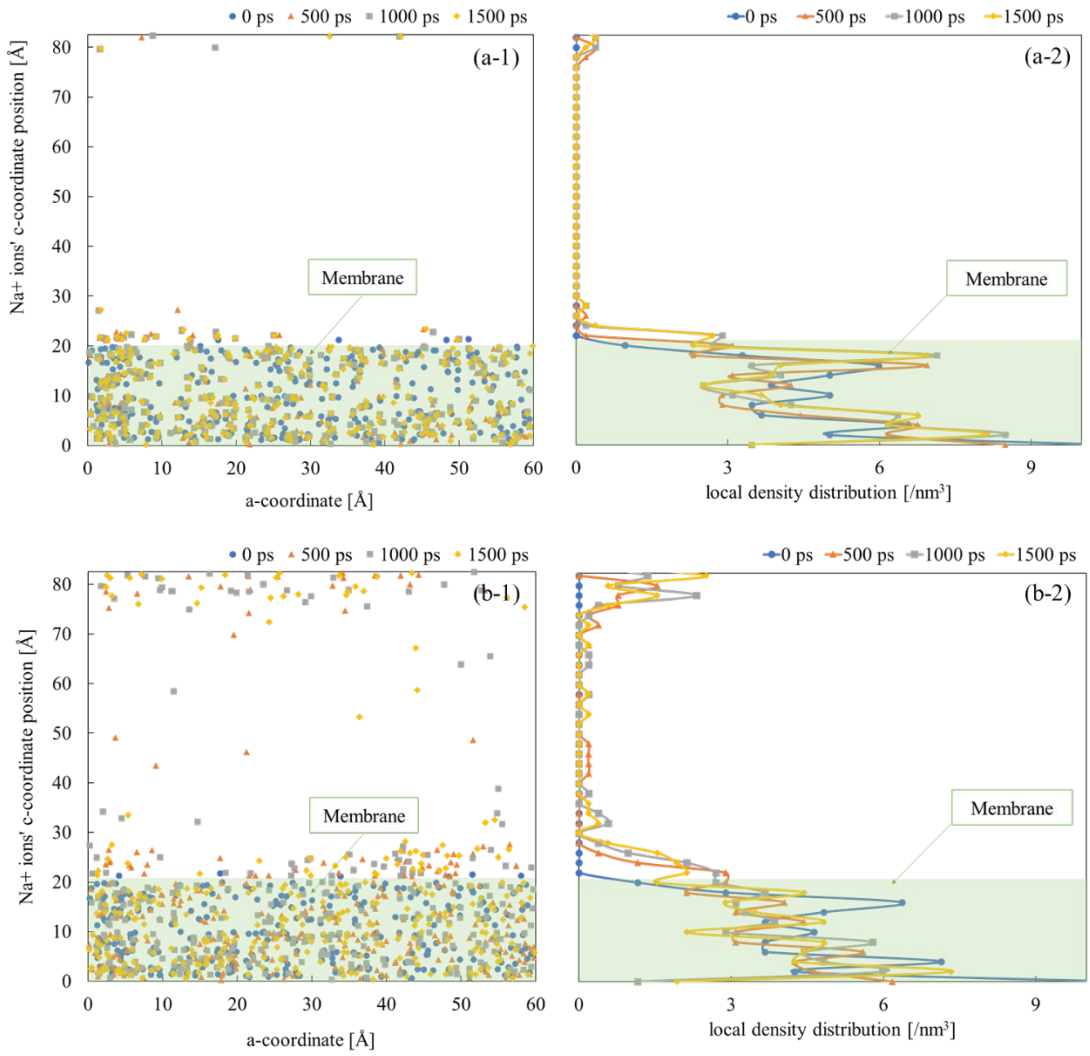

Fig. 5 The c-coordinate profiles and local density distribution of Na^+ ions in IPA (a-1, 2) and H_2O (b-1,2)

The behavior of Na^+ ions was different in H_2O and IPA. When the solvent was H_2O, Na^+ ions diffused from the inside of the membrane to the solvent. On the other hand, when the solvent was IPA, most of the Na^+ ions remained in the membrane. The remaining Na^+ ions in the case of IPA solvent moved or diffused slightly to the interface of the IPA and membrane and remained in the vicinity of the inside of the membrane surface. This suggests that cation exchange membranes with Na^+ ions as counter ions have a positive zeta potential in the IPA solvent because Na^+ ions accumulated near the membrane surface. Comparing the results at 1000 and 1500 ps, the position of Na^+ ions did not change significantly. Therefore, this simulation system reached an almost steady state and could express an actual state of the membrane-IPA interface.

3.3. *Effect of grafted chains: suppression of desorption*

The reason the SNP removal ratio was different among the three types of cation exchange membranes could be explained by the force curve in the AFM measurements. Fig. 6 shows the relative probability of the number of times the probe tip ruptured from the cation exchange membrane in the retract curve of one force curve measurement. Fig. 7 shows the recalculated relative probability of the number of ruptures with the horizontal axis set to the distance from the membrane surface when the rupture occurred. Note that the calculation of the relative probability includes the measurement results with zero ruptures. The rupture distances in Fig. 7 were 2.5 nm, and the relative probabilities were calculated from the number of ruptures in each range. The rupture distance was 0 nm when the number of ruptures was zero, but it was excluded from Fig. 7 for graph viewability.

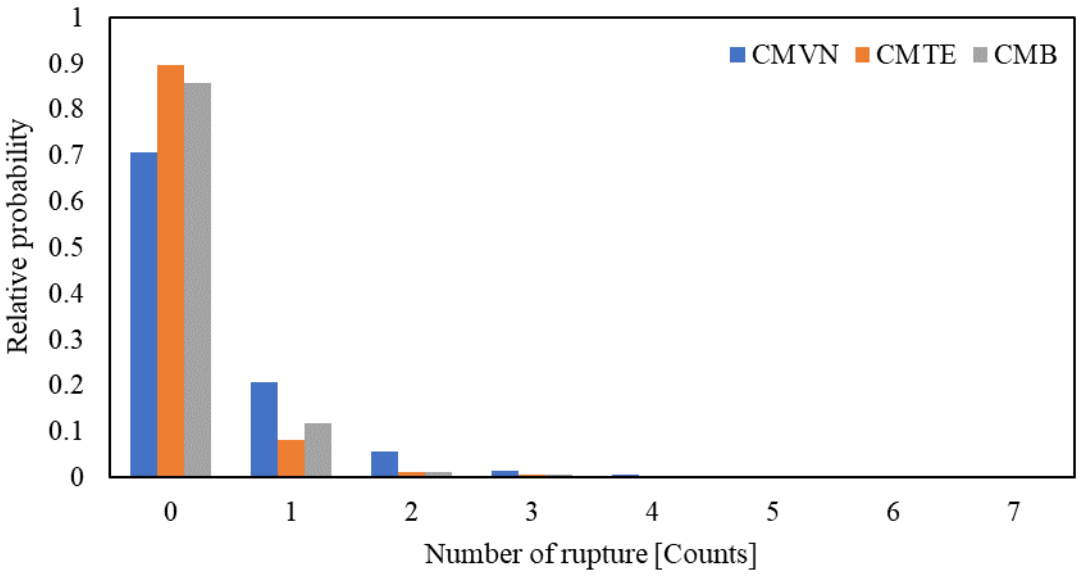

Fig. 6 Relationship between the number of ruptures and relative probability of each cation exchange membrane in the retract curves

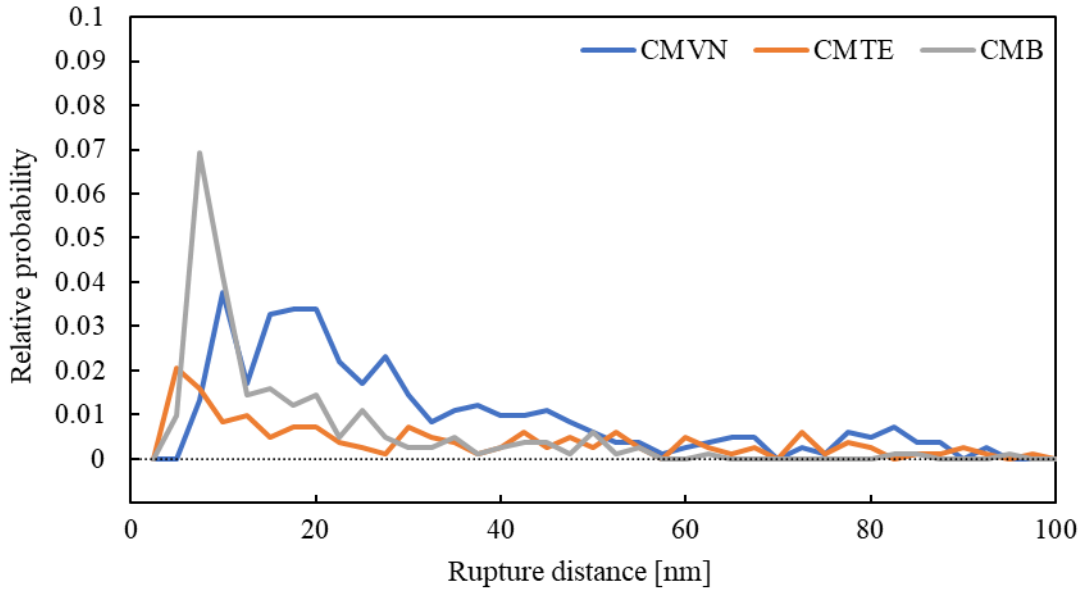

Fig. 7 Relationship between rupture distance and relative probability of each cation exchange membrane during retraction

The force curve measurements using AFM showed that the number of ruptures of CMVN was more than twice that of the other two membranes, suggesting that the cation exchange membrane interacts with the probe tip at multiple points. The rupture distance of CMVN was far from the membrane surface, indicating that its influence extends far. These results suggest that the grafted chains of CMVN contact the SNPs at multiple points and inhibit their desorption once adsorbed (tentacle effect [30–33]). The existence of these graft chains is the main reason for the difference in the removal ratio among the three types of cation exchange membranes. The removal ratio decreased with increasing SNP particle size; it was assumed that the particle size was larger than the distance affected by the graft chain.

4. Conclusion

This study examined the mechanism of SNP removal in pure IPA using cation exchange membranes through removal tests, zeta potential measurements, MD simulations, and AFM measurements. Among the three types of cation exchange membranes, CMVN had the highest removal ratio, and as the SNP size was increased, the removal ratios decreased for the cation exchange membranes. The removal test using AMVN, an anion exchange membrane with grafted chains and CMVN, showed no removal performance. This is consistent with the author's previous report. The zeta potential in IPA was measured first to examine the removal test results in more detail. The zeta potential of the cation exchange membrane in IPA was positive, which could explain the removal of SNPs with a negative zeta

potential in IPA. MD simulations were performed to examine why a cation exchange membrane with a negative zeta potential in water reversed to a positive one in IPA. The Na^+ ions in the membrane diffused to the bulk side when the solvent molecule was H_2O. However, when the solvent molecule was IPA, they moved from inside the membrane to near the membrane surface and remained there. This can explain the positive zeta potential of the cation exchange membrane in IPA. The reason for the difference in removal ratios among the three cation exchange membranes was assessed using AFM measurements of the cation exchange membrane in IPA. The number of ruptures and rupture distance obtained from the AFM measurements indicated that the grafted chains had a tentacle effect on the SNPs. This effect inhibited SNP desorption and explained why CMVN had the highest removal ratio. The results of this paper are expected to contribute to the development of filters with a membrane structure appropriate for removing impurities from organic solvents.

References

[1] G.E. Moore, Cramming more components onto integrated circuits, Reprinted from Electronics, volume 38, number 8, April 19, 1965, pp.114 ff., IEEE Solid-State Circuits Soc. Newsl. 11 (2006) 33–35. https://doi.org/10.1109/N-SSC.2006.4785860.

[2] D.I. Bae, B.D. Choi, Short channels and mobility control of GAA multi stacked nanosheets through the perfect removal of SiGe and post treatment, Electron. Lett. 56 (2020) 400–402. https://doi.org/10.1049/el.2019.3459.

[3] S. Rachidi, V. Loup, A. Campo, J.-M. Hartmann, N. Posseme, Wet Alkaline Etching of Si Selectively to SiGe for sub 10 nm Gate All Around Architectures, ECS J. Solid State Sci. Technol. 10 (2021) 14007. https://doi.org/10.1149/2162-8777/abddd8.

[4] P. Vimala, T.S.A. Samuel, A simulation study on the impact of InP barrier on InGaAs/InP hetero junction gate all around MOSFET, J. Nano Res. 60 (2019) 113–123. https://doi.org/10.4028/www.scientific.net/JNanoR.60.113.

[5] P.E. Raynal, V. Loup, L. Vallier, N. Bernier, J.M. Hartmann, P. Besson, WET and Siconi® cleaning sequences for SiGe epitaxial regrowth, Mater. Sci. Eng. B Solid-State Mater. Adv. Technol. 262 (2020) 114696. https://doi.org/10.1016/j.mseb.2020.114696.

[6] N. Sharma, N. Garg, G. Kaur, Performance analysis of gate stacked with nitride GAA-TFET, Mater. Today Proc. 28 (2020) 1683–1689. https://doi.org/10.1016/j.matpr.2020.05.128.

[7] M. Joodaki, Uprising nano memories: Latest advances in monolithic three dimensional (3D) integrated Flash memories, Microelectron. Eng. 164 (2016) 75–87. https://doi.org/10.1016/j.mee.2016.07.009.

[8] R. Micheloni, L. Crippa, C. Zambelli, P. Olivo, Architectural and integration options for 3D NAND flash memories, Computers. 6 (2017) 1–19.

https://doi.org/10.3390/computers6030027.
[9] P. Kumar, B. Raj, Parametric investigation and design of junctionless nanowire tunnel field effect transistor, Silicon. (2021). https://doi.org/10.1007/s12633-021-01371-2.
[10] J. Marra, J.A.M. Huethorst, Physical principles of Marangoni drying, Langmuir. 7 (1991) 2748–2755. https://doi.org/10.1021/la00059a057.
[11] L. Wilhelmy, Ueber die Abhängigkeit der Capillaritäts-Constanten des Alkohols von Substanz und Gestalt des benetzten festen Körpers, Ann. Der Phys. Und Chemie. 195 (1863) 177–217. https://doi.org/10.1002/andp.18631950602.
[12] J.A. Britten, A moving-zone Marangoni drying process for critical cleaning and wet processing, Solid State Technol. 40 (1997) 143+. https://link.gale.com/apps/doc/A20085177/AONE?u=anon~87a6a957&sid=googleScholar&xid=e038965c.
[13] T. Ohmi, S. Sudoh, H. Mishima, Static charge removal with IPA solution, IEEE Trans. Semicond. Manuf. 7 (1994) 440–446. https://doi.org/10.1109/66.330281.
[14] H. Mishima, T. Yasui, T. Mizuniwa, M. Abe, T. Ohmi, Particle-free wafer cleaning and drying technology, IEEE Trans. Semicond. Manuf. 2 (1989) 69–75. https://doi.org/10.1109/66.29672.
[15] IRDS, International Roadmap for Devices and Systems 2020 Edition Yield Enhancement, 2020 ed., IEEE, 2020. https://irds.ieee.org/editions/2020/yield-enhancement.
[16] Y. Fujimura, T. Kawakatsu, K. Nakagawa, T. Shintani, T. Yoshioka, Mechanism of silica nanoparticles removal in an isopropyl alcohol/water solution with an anion exchange membrane, J. Mol. Liq. 347 (2022) 118366. https://doi.org/10.1016/j.molliq.2021.118366.
[17] H. Sun, COMPASS: An ab initio force-field optimized for condensed-phase applicationsoverview with details on alkane and benzene compounds, J. Phys. Chem. B. 102 (1998) 7338–7364. https://doi.org/10.1021/jp980939v.
[18] H. Sun, Z. Jin, C. Yang, R.L.C. Akkermans, S.H. Robertson, N.A. Spenley, S. Miller, S.M. Todd, COMPASS II: extended coverage for polymer and drug-like molecule databases, J. Mol. Model. 22 (2016) 47. https://doi.org/10.1007/s00894-016-2909-0.
[19] H. Moradi, H. Azizpour, H. Bahmanyar, M. Mohammadi, M. Akbari, Prediction of methane diffusion coefficient in water using molecular dynamics simulation, Heliyon. 6 (2020) e05385. https://doi.org/10.1016/j.heliyon.2020.e05385.
[20] J.Y. Wu, Q.L. Liu, Y. Xiong, A.M. Zhu, Y. Chen, Molecular simulation of water/alcohol mixtures' adsorption and diffusion in zeolite 4a membranes, J. Phys. Chem. B. 113 (2009) 4267–4274. https://doi.org/10.1021/jp805923k.
[21] D. Rigby, Fluid density predictions using the COMPASS force field, Fluid Phase Equilib. 217 (2004) 77–87. https://doi.org/10.1016/j.fluid.2003.08.019.
[22] B. Thomson, A. Rudin, G. Lajoie, Dispersion copolymerization of styrene and divinylbenzene: Synthesis of monodisperse, uniformly crosslinked particles, J. Polym. Sci. A Polym. Chem. 33 (1995) 345–357. https://doi.org/10.1002/pola.1995.080330301.

[23] W. Yang, W. Ming, J. Hu, X. Lu, S. Fu, Morphological investigations of crosslinked polystyrene microspheres by seeded polymerization, Colloid Polym. Sci. 276 (1998) 655–661. https://doi.org/10.1007/s003960050294.

[24] M. Sangkhawasi, T. Remsungnen, A.S. Vangnai, R.P. Poo-Arporn, T. Rungrotmongkol, All-Atom Molecular Dynamics Simulations on a Single Chain of PET and PEV Polymers, Polymers (Basel). 14 (2022) 1–11. https://doi.org/10.3390/polym14061161.

[25] K. Wang, H. Li, J. qiang Li, H. xiang Xu, C. Zhang, Y. ying Lu, X. zhong Fan, W. qiang Pang, Molecular dynamic simulation of performance of modified BAMO/AMMO copolymers and their effects on mechanical properties of energetic materials, Sci. Rep. 10 (2020) 1–17. https://doi.org/10.1038/s41598-020-75146-x.

[26] H.J.C. Berendsen, J.P.M. Postma, W.F. van Gunsteren, A. DiNola, J.R. Haak, Molecular dynamics with coupling to an external bath, J. Chem. Phys. 81 (1984) 3684–3690. https://doi.org/10.1063/1.448118.

[27] V.I. Kuchuk, I.Y. Shirokova, E. V Golikova, Physicochemical properties of water-alcohol mixtures of a homological series of lower aliphatic alcohols, Glas. Phys. Chem. 38 (2012) 460–465. https://doi.org/10.1134/S1087659612050057.

[28] F.-M. Pang, C.-E. Seng, T.-T. Teng, M.H. Ibrahim, Densities and viscosities of aqueous solutions of 1-propanol and 2-propanol at temperatures from 293.15 K to 333.15 K, J. Mol. Liq. 136 (2007) 71–78. https://doi.org/10.1016/j.molliq.2007.01.003.

[29] J.-G. Park, S.-H. Lee, J.-S. Ryu, Y.-K. Hong, T.-G. Kim, A.A. Busnaina, Interfacial and electrokinetic characterization of ipa solutions related to semiconductor wafer drying and cleaning, J. Electrochem. Soc. 153 (2006) G811. https://doi.org/10.1149/1.2214532.

[30] S. Tsuneda, H. Kagawa, K. Saito, T. Sugo, Hydrodynamic evaluation of three-dimensional adsorption of protein to a polymer chain grafted onto a porous substrate, J. Colloid Interface Sci. 176 (1995) 95–100. https://doi.org/10.1006/jcis.1995.0011.

[31] L. Zhao, C. Liang, S. Li, K. Du, Study of tentacle-like cationic macroporous cellulose spherical adsorbent for heavy metals, J. Clean. Prod. 303 (2021) 127114. https://doi.org/10.1016/j.jclepro.2021.127114.

[32] C. Aydoğan, K. Çetin, A. Denizli, Novel tentacle-type polymer stationary phase grafted with anion exchange polymer chains for open tubular CEC of nucleosides and proteins, Analyst. 139 (2014) 3790–3795. https://doi.org/10.1039/C3AN01897K.

[33] S. Tsuneda, K. Saito, S. Furusaki, T. Sugo, High-throughput processing of proteins using a porous and tentacle anion-exchange membrane, J. Chromatogr. A. 689 (1995) 211–218. https://doi.org/10.1016/0021-9673(94)00911-R.